MATERIALS SCIENCE

MXenes stretch hydrogel sensor performance to new limits

Yi-Zhou Zhang[1]*, Kang Hyuck Lee[1]*, Dalaver H. Anjum[2], Rachid Sougrat[2], Qiu Jiang[1], Hyunho Kim[1], Husam N. Alshareef[1]†

The development of wearable electronics, point-of-care testing, and soft robotics requires strain sensors that are highly sensitive, stretchable, capable of adhering conformably to arbitrary and complex surfaces, and preferably self-healable. Conductive hydrogels hold great promise as sensing materials for these applications. However, their sensitivities are generally low, and they suffer from signal hysteresis and fluctuation due to their viscoelastic property, which can compromise their sensing performance. We demonstrate that hydrogel composites incorporating MXene ($Ti_3C_2T_x$) outperform all reported hydrogels for strain sensors. The obtained composite hydrogel [MXene-based hydrogel (M-hydrogel)] exhibits outstanding tensile strain sensitivity with a gauge factor (GF) of 25, which is 10 times higher than that of pristine hydrogel. Furthermore, the M-hydrogel exhibits remarkable stretchability of more than 3400%, an instantaneous self-healing ability, excellent conformability, and adhesiveness to various surfaces, including human skin. The M-hydrogel composite exhibits much higher sensitivity under compressive strains (GF of 80) than under tensile strains. We exploit this asymmetrical strain sensitivity coupled with viscous deformation (self-recoverable residual deformation) to add new dimensions to the sensing capability of hydrogels. Consequently, both the direction and speed of motions on the hydrogel surface can be detected conveniently. Based on this effect, M-hydrogel demonstrates superior sensing performance in advanced sensing applications. Thus, the traditionally disadvantageous viscoelastic property of hydrogels can be transformed into an advantage for sensing, which reveals prospects for hydrogel sensors.

INTRODUCTION

Hydrogels comprise an interesting class of viscoelastic materials that are composed of three-dimensional (3D) networks of hydrophilic polymers that are cross-linked, chemically or physically, with the capacity to absorb and retain a large amount of water. Conductive hydrogels have recently emerged as promising materials for applications such as wearable electronics, soft robotics, and prosthetics. These applications require sensors to be highly sensitive, stretchable, and easy to adhere to arbitrary and complex surfaces, such as human skin (*1*–*4*). However, hydrogel-based electromechanical sensors generally exhibit relatively low sensitivity, and as viscoelastic materials, their electromechanical responses to external forces convey unstable noises with hysteresis and fluctuation due to unexpected viscous deformations (*5*–*7*). Recently, researchers have used a special class of conductive nanofillers, whose geometry and conductivity can both be changed by deformations, to improve the sensitivity of strain sensors (*8*–*12*). Although these nanofiller networks can improve sensitivity, they still cannot overcome the limitations that originate from viscous deformations (*9*, *13*). In addition, these nanofillers usually cannot maintain their deformed network structure because of their easy motion within the hydrogel matrix and possible rearrangement of the network structure by an electric field (*14*). This consequently compromises sensing reliability.

MXenes refer to a booming class of 2D early-transition metal carbides/carbonitrides that have hydrophilic surfaces and high electrical conductivity (*15*, *16*), which renders them promising for applications such as electrochemical energy storage devices (*17*–*20*). Recently, MXenes have been demonstrated to be potentially useful materials for electromechanical sensors with high strain sensitivity because of the substantial change in interlayer distance in response to external pressure in addition to their favorable mechanical properties (*21*, *22*). Here, we propose MXenes as conductive fillers in hydrogels because, in addition to their high strain sensitivity, MXene nanosheets have abundant surface functional groups (–OH, –F, –O, etc.), which produce negatively charged hydrophilic surfaces (*23*). These surfaces can significantly improve the mechanical properties of hydrogels, such as elastic modulus and stretchability, through the formation of a unique clay-polymer network structure that is cross-linked with uniformly dispersed clays and densely entangled polymer chains (*24*–*26*). Furthermore, the high density of surface functional groups, such as –OH, can increase the number of hydrogen bonds in the hydrogel system, thereby improving the self-healability of hydrogels (*27*).

Here, we demonstrate for the first time that MXene-based hydrogel (M-hydrogel) exhibits extremely high stretchability, instantaneous self-healability, and excellent conformability and adhesiveness to various surfaces, including human skin. The performance of the M-hydrogel–based sensor exceeds that of all previously reported hydrogel strain sensors. The preparation method is simple and involves mixing MXene ($Ti_3C_2T_x$) nanosheets with a commercial low-cost hydrogel that is commonly used in toys, namely "crystal clay," which is composed of poly(vinyl alcohol) (PVA), water, and antidehydration additives. We show that the addition of MXene nanosheets can significantly improve the strain sensitivities of hydrogel, and we demonstrate that M-hydrogel exhibits much higher sensitivity under compressive strains than under tensile strains. As a result of the asymmetrical strain sensitivity and viscous deformations (self-recoverable residual deformation), the M-hydrogel sensor presents distinguishable, resistance-dependent patterns from a series of deformations that occur when an object moves on its surface. On the basis of this mechanism, M-hydrogel can conveniently detect both the direction and speed of motions without a complex circuit design. These unique sensing characteristics have not been

[1]Physical Sciences and Engineering Division, Materials Science and Engineering Department, King Abdullah University of Science and Technology (KAUST), Thuwal 23955-6900, Kingdom of Saudi Arabia. [2]KAUST, Imaging and Characterization Core Lab, Thuwal 23955-6900, Kingdom of Saudi Arabia.
*These authors contributed equally to this work.
†Corresponding author. Email: husam.alshareef@kaust.edu.sa

previously used to add extra dimensions to the sensing capability of strain sensors.

RESULTS

Titanium carbide MXene ($Ti_3C_2T_x$) nanosheets were prepared through etching and delamination of a layered metal carbide precursor known as MAX (Ti_3AlC_2) in accordance with a previous report (*28*) (fig. S1A), thus producing MXene nanosheets in the size range of 1 to 5 μm (Fig. 1A, left). The high quality of the obtained MXene nanosheets was proven by high-resolution transmission electron microscopy (HRTEM; Fig. 1A, upper right and lower right), Raman spectroscopy (fig. S1B), and x-ray diffraction (XRD; fig. S1C). The obtained MXene nanosheets were manually mixed with a commercial hydrogel, crystal clay, which contains PVA, water, and antidehydration additives. The obtained M-hydrogel exhibits impressive stretchability, as Fig. 1B illustrates. A rectangular piece of M-hydrogel with a length of 2.5 cm can be easily stretched to more than 86 cm, which translates to a stretchability of at least 3400% (Fig. 1B and movie S3). In comparison, the same volume of pristine hydrogel can only be stretched to 55 cm at most, which indicates a maximum stretchability of less than 2200% (fig. S2A and movie S4). This improvement can be attributed to the creation of secondary cross-linking upon the addition of MXene nanosheets with negatively charged surfaces (*23*) into the hydrogel system. This can lead to the homogeneous dispersion of negatively charged nanosheets into the polymer network and narrow length distribution of polymer chains between the nanosheets (*26*). This yields a densely entangled polymer network structure (fig. S3A), which increases the elastic modulus, elongation to break, and toughness of the composite hydrogel (*24*–*26*). M-hydrogel also exhibits instantaneous self-healability, as two pieces of the M-hydrogel demonstrated the same stretchability before being cut as they did once they were gently reattached (Fig. 1C and movie S1). In comparison, necking emerges at the reconnected interface of two cut pieces of the pristine hydrogel under stretching, followed by mechanical failure at the necking point (fig. S2B and movie S2). The self-healing property of PVA hydrogel derives from the hydrogen bonding between the –OH groups (*27*). By adding MXene into the PVA hydrogel, the abundant surface functional groups can provide additional hydrogen bonding sites (fig. S3B), which, in turn, enhance self-healability.

To understand the 3D network structure of MXene nanosheets in the hydrogel matrix, 3D TEM tomography was conducted. This method uses a series of TEM images of M-hydrogel (thickness of 100 nm; Fig. 1D) that are captured with varying tilt angles from −68° to +68° at two-degree intervals (movie S5) and with a depth of focus ranging from −50 to 50 nm (movie S6). It is clear that MXene nanosheets in the hydrogel matrix adopt random spatial orientations, and most interconnections between nanosheets exhibit surface-edge characteristics (Fig. 1, E and F).

The electromechanical responses of the M-hydrogel to tensile and compressive deformations have been characterized (Fig. 2, A and B). Under tensile deformation, the resistance increases, and the fractional resistance change ($R - R_0/R_0$) of M-hydrogel heightens with increasing strain. Moreover, the sensitivity defined as the gauge factor (GF = $\Delta R/R_0 \cdot \varepsilon$) of the M-hydrogels increases from 2 to 25 as the MXene weight percentage increases from 0 to 4.1% (Fig. 2A, inset). This sensitivity is substantially higher than that of other reported hydrogel-based strain sensors (*8*, *12*, *29*–*33*). Table S1 shows a comparison of the GF of our M-hydrogel sensor with those of recently reported hydrogel strain sensors. M-hydrogel exhibits significantly more sensitive electromechanical responses under compression, as Fig. 2B illustrates. The corresponding GFs are 60 to 80 in the compressive strain range of

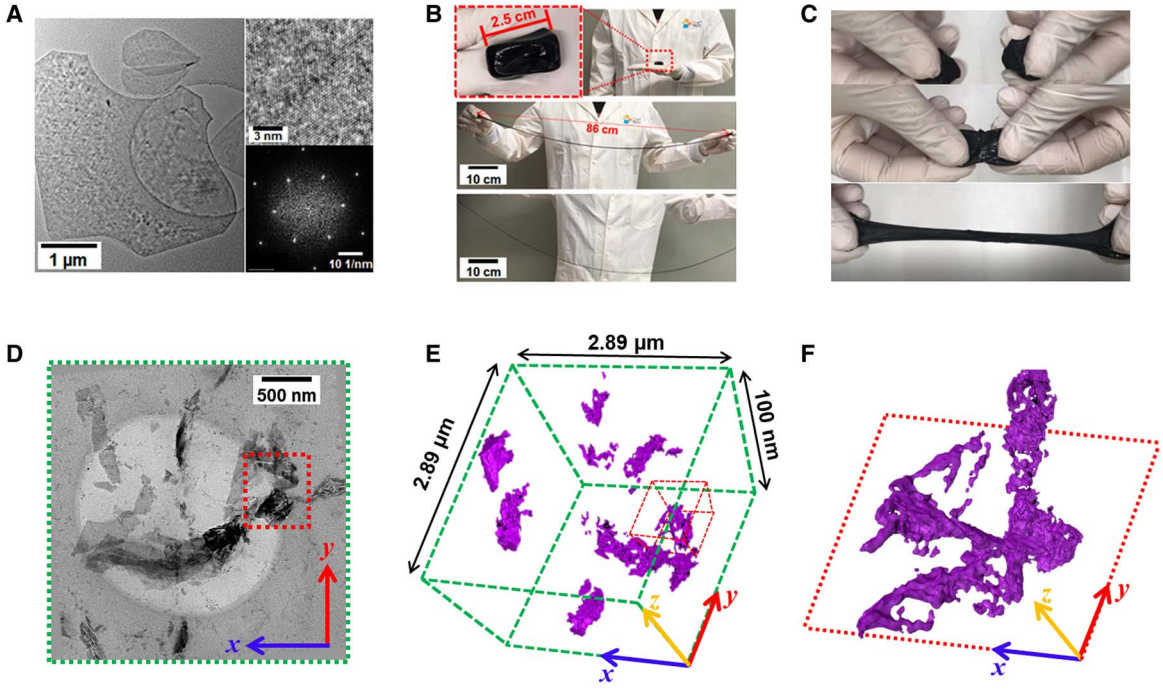

Fig. 1. Characterizations of M-hydrogel. (**A**) Transmission electron microscopy (TEM) of MXene nanosheets; shown in the upper right is the HRTEM image of a typical nanosheet, and shown in the lower right is the corresponding fast Fourier transform (FFT). (**B**) Photographs demonstrating the stretchability of M-hydrogel. (**C**) Photographs depicting the self-healing capability of the M-hydrogel: two cut pieces (top), once gently touched (middle), and showing retention of the original stretchability of M-hydrogel (bottom). (**D**) TEM image of M-hydrogel. (**E**) 3D tomography image based on the entire area in (D) and (**F**) zoomed-in 3D tomography image of a selected volume marked with red box in (E).

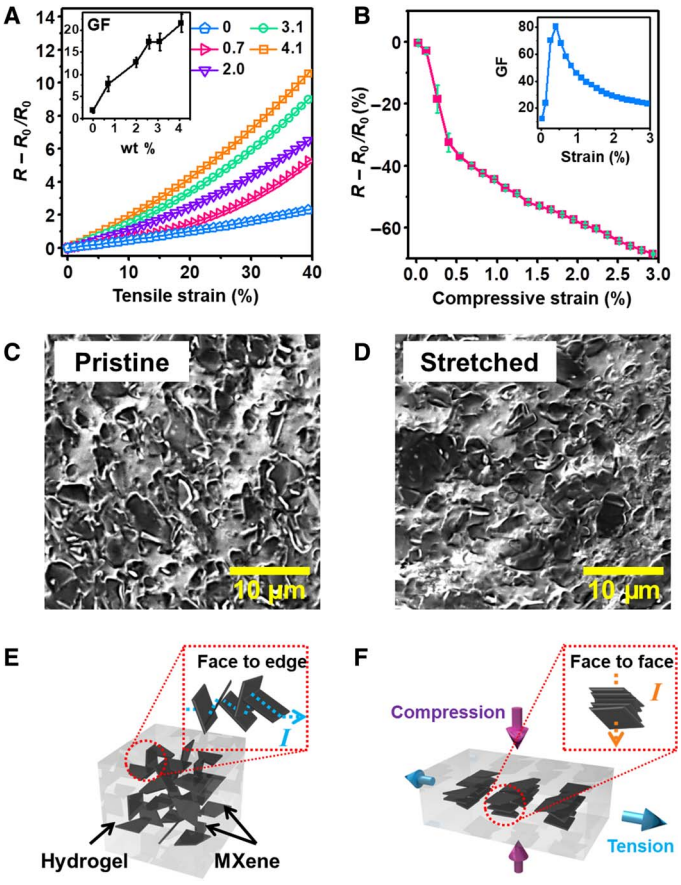

Fig. 2. Electromechanical properties of M-hydrogel composite and mechanisms. (**A** to **F**) Electrical response of M-hydrogel to (A) tensile strain and (B) compressive strain, with insets showing the corresponding GFs; scanning electron microscopy (SEM) images of M-hydrogel surface (C) before and (D) after stretching; and (E and F) a schematic illustration of the mechanism of the electromechanical responses of M-hydrogel. wt %, weight %.

0 to 0.5%, but they decrease from 80 to 21 in the strain range of 0.5 to 3% (Fig. 2B, inset). This performance reveals a trend and GF value (80 at 0.5% strain) that are comparable to those of the recently reported MXene thin film–based piezoresistive sensor (94.8 at 0.82% strain), the resistance of which changes because of reduced contact resistance between MXene sheets induced by compression (*21*).

We mainly attribute the significant differences in electromechanical properties under tensile and compressive deformation in M-hydrogel to the 3D network structure of the MXene nanosheets embedded within the hydrogel matrix. Under tensile deformation, the resistance increases as a result of the geometry of the M-hydrogel, wherein the spacing between the MXene nanosheets increases and consequently reduces their chances of making contact in the hydrogel matrix. In contrast, under compressive deformation, the geometry of the M-hydrogel becomes shorter, ultimately leading to less separation between MXene sheets and improving the likelihood of the MXene nanosheets making contact. As a further result, the M-hydrogel resistance decreases. Moreover, as SEM characterization has indicated, the surface morphology of M-hydrogel exhibits a high concentration of protruding MXene nanosheets due to their randomly oriented 3D network structure (Fig. 2C). However, the number of protruding nanosheets evidently decreases when the M-hydrogel is laterally stretched (Fig. 2D). Thus, compression not only prompts geometrical changes and an increase in interconnection points but also transforms face-to-edge interconnections into face-to-face interconnections, as Fig. 2 (E and F) demonstrates. Increasing compressive strain further reduces the gaps between the face-to-face interconnected MXene nanosheets, and more surface contacts are established between MXene sheets. For these reasons, compressive deformation has a more marked impact than tensile deformation on the resistance of the hydrogel.

We demonstrated the viscoelastic property of M-hydrogel by testing its electric response to local deformation (fig. S5A). When we pushed a polydimethylsiloxane tip against the M-hydrogel surface, the resistance increased as a result of the geometric effect due to the immersed tip, as fig. S5B (blue curve) demonstrates. At low speed, the deformation could be fully recovered (fig. S5D, orange and blue curves); however, when the pushing speed was increased, the resistance could not recover its initial value because of the formation of residual deformation (fig. S5C, inset) under high-speed movement (fig. S5D, red curve). This phenomenon is due to the viscoelastic property of materials such as hydrogels, and it is usually considered a disadvantage of their application in strain sensors.

However, when combined with the anisotropic response to compressive and tensile strains, it is possible to observe interesting sensing capabilities using the M-hydrogel. To test this, we first measured the resistance change of M-hydrogel while a spherical object moved along its surface. We defined the direction of the electric current as the *x* axis and the direction vertical to the electric current on the M-hydrogel surface as the *y* axis [Fig. 3 (A and B), inset schematics]. The resistance increased when the object moved in the *y* direction (Fig. 3A). Conversely, the resistance decreased when the object moved in the *x* direction (Fig. 3B). We attribute this phenomenon to the anisotropic response of M-hydrogel to tensile and compressive strains, as discussed in the previous paragraph (that is, movement in *x* direction exerts predominantly compressive strain that reduces resistance, whereas movement in *y* direction exerts a predominantly tensile strain that increases resistance). To test this hypothesis, we measured the resistance change of the M-hydrogel undergoing the same amount of tensile and compressive deformation (Fig. 3C and fig. S6). When a conducting copper plate was moved along the M-hydrogel surface to either side in the *x* direction (Fig. 3C, inset), the resistance of the M-hydrogel was reduced, which indicates that motion in the *x* direction induces a predominantly compressive strain response. In comparison, motion along both the *x* and *y* axes yielded increased resistance on the pristine hydrogel surface (fig. S7, A and B). This sensitivity to motion directions can be used for electronic skin applications. To demonstrate, we have determined that the M-hydrogel can distinguish between a rectangular trace (fig. S7C) and a circular trace (fig. S7D) left by motions on the surface of M-hydrogel, whereas pristine hydrogel cannot (fig. S7, E and F).

Apart from movement direction, M-hydrogel can also sense motion speed, as evidenced by a model experiment in which we rolled a cylinder down a slope with the M-hydrogel surface (Fig. 3D). The mean velocity of the cylinder passing through the M-hydrogel surface was controlled by the initial position of the object on the slope. The resistance change of M-hydrogel exhibited three distinct regions as the object (cylinder) was rolled down its surface (Fig. 3E). The resistance change curve first displayed upward peaks when the rolling cylinder reached the M-hydrogel (region "I"), which is similar to the response obtained from vertical deformation (fig. S5 and Fig. 3A). The resistance change curve then exhibited a wide downward peak (region "II"), which

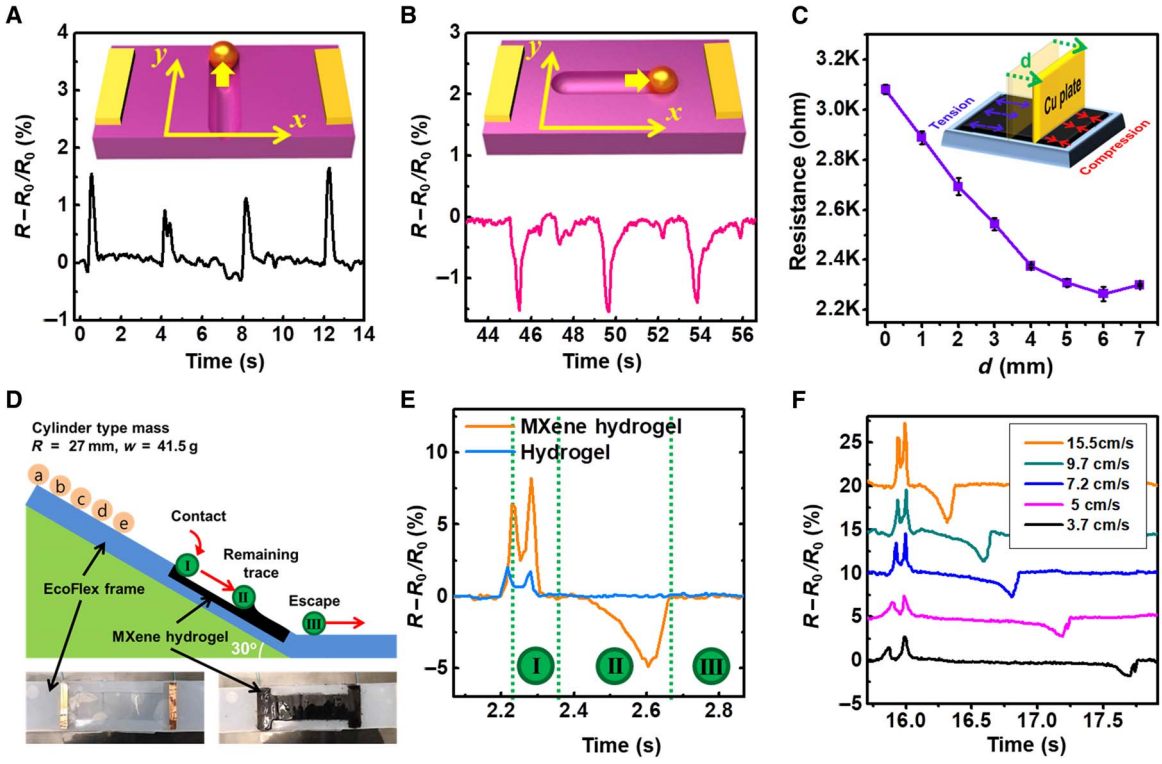

Fig. 3. Sensing capability of M-hydrogel to motions on its surface. Resistance change of M-hydrogel in response to motion on its surface (A) vertical to the current direction and (B) parallel to the current direction. (**C**) Experimental setup to explain the motion direction sensing capability of M-hydrogel and corresponding result. (**D**) Schematic for motion speed sensing. (**E**) Speed sensing result comparison between M-hydrogel and pristine hydrogel. (**F**) Motion sensing of M-hydrogel in response to different motion speeds.

corresponds to the velocity of the rolling cylinder exceeding the relaxation speed (fig. S8). Finally, M-hydrogel returned to the initial resistance value after the rolling cylinder escaped from the M-hydrogel surface. As the mean velocity of the object increased, the peak height in region II rose, and the span of the region II decreased (Fig. 3F). In comparison, pristine hydrogel does not present peaks in the region II (Fig. 3E, blue curve), which reinforces the role of MXene in speed sensing. The unique response of the M-hydrogel to motion speed and direction indicates interesting and promising sensing capabilities from the addition of MXene nanoflakes into the hydrogel matrix, especially for complex and subtle motions.

Next, we demonstrate for the first time that the M-hydrogel can be used as a sensing material to detect various bodily motions (hand gestures and facial expressions) and to monitor vital signals (human pulse). Because of its uniquely soft, sticky, and stretchable characteristics, M-hydrogel can readily adhere to various positions on the human body with complex 3D geometry (hand, neck, face, etc.) without adhesives. First, M-hydrogel was attached to the index finger and reflected a 20% resistance change when the finger was bent. The signal was clear and stable under both fast and slow bending motions (Fig. 4A). More complex gestures involving full hand motions were readily detected by adhering the M-hydrogel to the knuckle. The gestures for "zero," "one," "two," "three," "four," and "five" each yielded a distinct resistance value, and the signals were fully recoverable, as Fig. 4B demonstrates. When mounted over the carotid artery, delicate waveforms that depict the pulse with a characteristic double peak and dicrotic notch along with other fingerprint signals that allow for accurate pulse monitoring (Fig. 4C) were detected. When adhered to the middle of the forehead, facial expressions, such as smiling and frowning, could be distinguished (Fig. 4, D and E).

M-hydrogel's unique capabilities for sensing motion speed and direction as discussed above have enabled certain advanced sensing applications. First, M-hydrogel was used as the sensing film for signature recognition (Fig. 5A). Because individual handwriting involves a set of unique characteristics, including the force, speed, and sequence of the writing, M-hydrogel produces a complex and unique waveform for even a simple signature (Fig. 5B). Even the same simple word "OK" exhibits significantly different waveforms when written by two individuals (Fig. 5, C and D). In comparison, pristine hydrogel yields similar pattern of signals for OK when written by the same two test subjects (fig. S9, A and B), which reflects a remarkable potential of M-hydrogel for anticounterfeiting applications. M-hydrogel has been further used to detect another vital signal that urgently requires accurate monitoring, namely the phonatory process (voicing). When attached to the laryngeal prominence, or "Adam's apple," M-hydrogel produces stable and unique patterns for the voices of test subjects. As Fig. 5 (F to H) indicates, even similarly sounding single syllables, such as "B," "D," and "E," produce easily distinguishable patterns that are superior to those of previous reports (*8*, *34*, *35*) and from pristine hydrogel (fig. S9, C to E). This result is due to the sensitivity of M-hydrogel to subtle vibrations related to the laryngeal prominence and surrounding skin. The impressive sensing capability of M-hydrogel on phonation via the electromechanical approach could present an opportunity for us to "hear" the vocally impaired.

DISCUSSION

In summary, we have developed an MXene ($Ti_3C_2T_x$)–based PVA hydrogel with excellent sensing capabilities. Adding MXene nanosheets

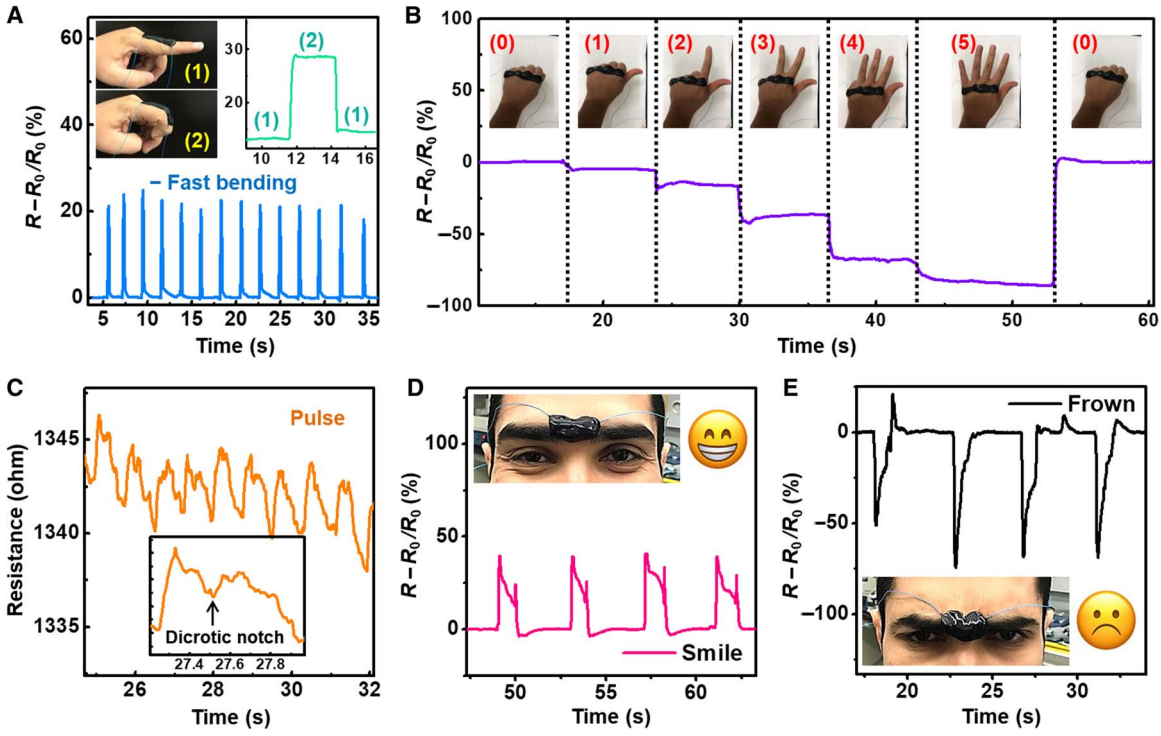

Fig. 4. General sensing performance of M-hydrogel. (**A** to **E**) Resistance change of M-hydrogel in response to (A) finger bending, (B) different hand gestures, (C) human pulse, and (D and E) facial expressions.

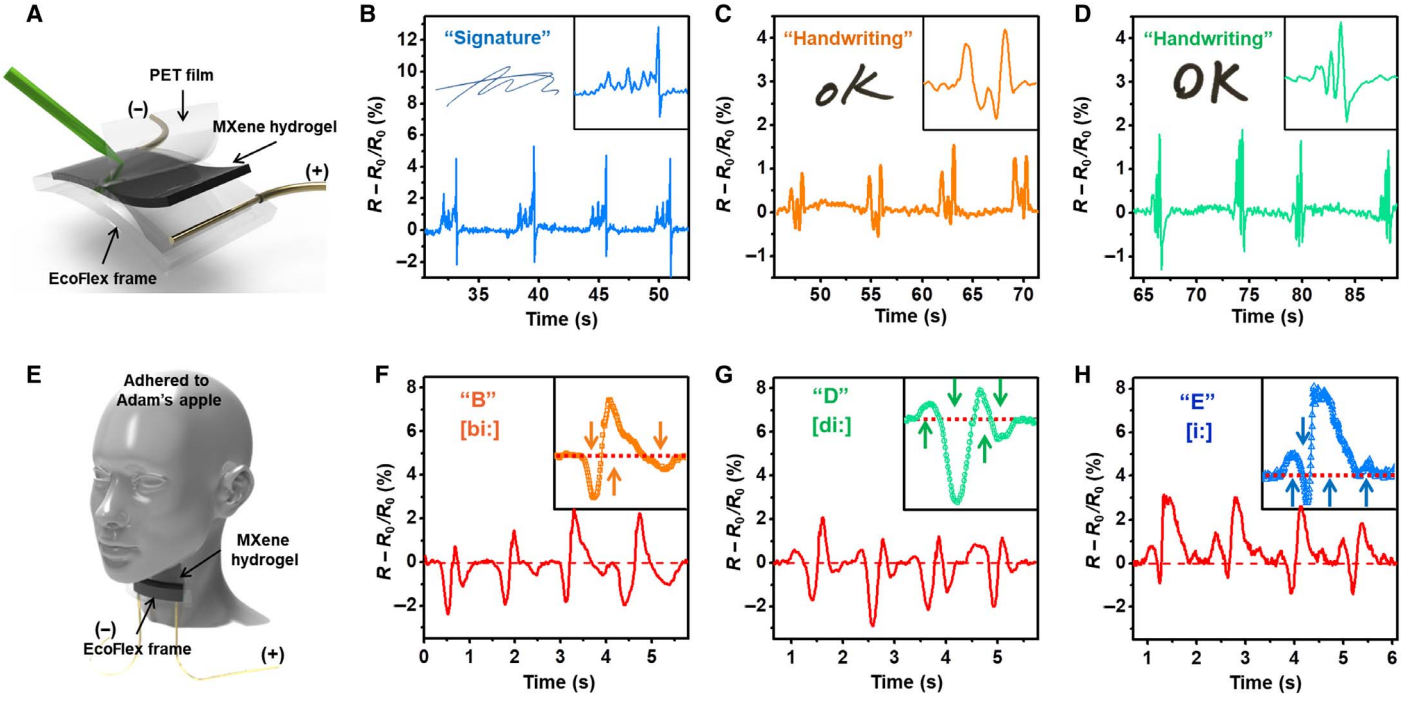

Fig. 5. Advanced sensing applications of M-hydrogel. (**A**) Schematic for signature sensing. (**B** to **D**) Resistance change to (B) signature and (C and D) OK written by different volunteers. (**E**) Schematic for vocal sensing. (**F** to **H**) Resistance change in response to similarly sounding letters "B," "D," and "E."

with multiple surface functional groups into the PVA hydrogel can result in outstanding stretchability and instantaneous self-healability. The combination of the high sensitivity of MXene nanosheets, the anisotropic response of M-hydrogel to compressive and tensile strains, and its viscoelastic properties characterize the obtained composite hydrogel as an interesting sensing material that can conveniently detect motion direction and speed on its surface. Based on this effect, advanced sensing applications that involve subtle changes in motion speed and

traces, such as handwriting, facial expressions, and vocal signals, can all be detected with high accuracy and sensitivity.

The unique sensing capability demonstrated in this work can be extended to other sensing applications that involve 3D motions, including touch sensing and biosignal monitoring. With its excellent stretchability, adhesiveness, and conformability, M-hydrogel is a promising material for wearable electronics, soft robotics, and artificial skin. The simple fabrication method promises a whole range of composite hydrogel-based sensing materials.

MATERIALS AND METHODS

Synthesis of MXene ($Ti_3C_2T_x$) nanosheets and M-hydrogel

$Ti_3C_2T_x$ MXene was synthesized following the LiF/HCl method (*28*). The etching solution was prepared by adding 1.5 g of LiF to 10 ml of 6 M hydrochloric acid, followed by stirring for 5 min. Then, 2 g of Ti_3AlC_2 powder was slowly added to the etchant at 35°C and stirred for 24 hours. The acidic suspension was washed with deionized water until a pH value of 6 was reached via centrifugation at 3500 rpm (5 min per cycle) and decanting of the supernatant after each cycle. The MXene nanosheets were collected via centrifugation at 3500 rpm for 5 min.

The M-hydrogel was prepared in the following way: First, MXene paste was obtained from centrifugation at 8000 rpm for 60 min of the obtained MXene suspension and collecting the sediment. Second, MXene paste was spread on pristine crystal clay, the mixed hydrogel was then rolled into a ball and flattened by hand, and the process was repeated three to five times until the color of the mixture became uniformly black, as shown in Fig. 1B. The weight percentages of M-hydrogels were determined as the dried weight of MXenes divided by the total weight of the corresponding M-hydrogel.

Characterizations of MXene and M-hydrogel

The XRD patterns of MXene were measured with a powder XRD (Bruker, D8 ADVANCE) with Cu Kα radiation (λ = 0.15406 nm). The surface morphology of M-hydrogel samples was characterized with field-emission SEM of the model Nova NanoSEM from Thermo Fisher Scientific. The structure of the MXene nanosheets was studied with a TEM of the model Titan Themis Z, also from Thermo Fisher Scientific. The microscope was equipped with an image corrector to minimize the effect of spherical aberration on the TEM images. In this way, several low-magnification and higher-magnification images were acquired in bright-field TEM (BF-TEM) mode along with selected-area electron diffraction (SAED) patterns. The BF-TEM images revealed the size of the nanosheets to be several micrometers, while the SAED patterns confirmed the hexagonal crystal structure of MXene.

The 3D structure of M-hydrogel was investigated through the technique of electron tomography (ET) that is available in another TEM of the model Titan 80-300 CT, again from Thermo Fisher Scientific. ET experiments were performed in BF-TEM mode that acquired the tilt series by using the Xplore3D tomography software package. Note that the sample was tilted from −68° to +68°, and images were captured at two-degree initial intervals under the Saxton scheme. The acquired tomo series was then aligned and reconstructed with the Inspect 3D software package. It is pertinent that the simultaneous iterative reconstruction tomography scheme has been used to reconstruct the data sets to enhance the image contrast of volume slices (or tomograms). 3D rendering models were generated with the segmentation tools implemented in Avizo Fire 8.0 software. The Raman spectra were collected with a micro-Raman spectrometer (LabRAM Aramis) equipped with a long working distance 50× objective lens (LMPLFLN50X, Olympus) using a Cobolt laser (633 nm, 5 mW at source).

Electromechanical measurements

Electromechanical measurements for both tensile and compressive tests were performed on M-hydrogel (4.1 wt %) and pristine hydrogel samples using Keithley KE4200-SCS in the two-probe mode. The tensile samples were rolled into the desired shape with dimensions measured by electronic Vernier calipers. For electromechanical tensile tests, specimens with a gauge length of L_0 = 25 mm and a diameter of D_0 = 5 mm were strained at a rate of 0.2 mm/s until reaching tensile strain of ~45%. A syringe filled with M-hydrogel (4.1 wt %) was used for electromechanical compressive tests (fig. S2). The gauge length and diameter of the M-hydrogel in the syringe were 15 and 10 mm, respectively. The resistances were measured at steps of 0.2 mm with a diminishing gauge length. For electromechanical tests, contact was made by placing copper wire leads 5 mm inside each end of the sample.

M-hydrogel/pristine hydrogel–based mechanical sensors for bodily motion sensing

M-hydrogel with 4.1 wt % of MXene nanosheets was used to sense bodily motions. Both ends of the M-hydrogel were connected to Keithley KE4200-SCS via copper wires. To sense the finger-bending motion, 2.5 g of M-hydrogel was placed on the index finger as shown in the inset of Fig. 4A, and resistance changes were measured when the finger was repeatedly bent and released. For the detection of full hand gestures in Fig. 4B, 5 g of M-hydrogel was rolled into a rectangular shape (length × width × thickness of 120 mm × 15 mm × 3 mm) and adhered to the knuckle of a clenched fist. After that, the resistance change over time was monitored from each hand gesture. To measure human pulse, 2.5 g of M-hydrogel was mounted over the carotid artery of the neck of the test subject. The same amount of M-hydrogel was applied for the detection of facial expressions. M-hydrogel or pristine hydrogel was adhered to the middle of the forehead of the volunteer, and the resistance change was measured from repeated smiling and frowning expressions, which were maintained for about 2 s at an interval of approximately 5 s.

M-hydrogel/pristine hydrogel–based sensors for signature and vocal recognition

First, an EcoFlex frame (length × width × thickness is 180 mm × 45 mm × 3 mm) with a central cavity (105 mm × 15 mm × 1 mm) was fabricated to contain M-hydrogel (4.1 wt %) and pristine hydrogel, respectively. The EcoFlex frame was adopted to confine hydrogels during testing, thereby improving the sensing reliability. Two copper-pad electrodes with a size of 15 mm × 5 mm were fixed to the ends of the cavity to ensure stable contact between hydrogels and Keithley KE4200-SCS, connected by copper wires. A polyethylene terephthalate (PET) film of 0.1-mm thickness protected the hydrogels to prevent mechanical failure and reduce friction force from the pencil during writing (Fig. 5A). Hydrogels contained in the same EcoFlex frame were used for vocal recognition without the PET protection film. These sensors were attached to the laryngeal prominence with the skin exposed to the surface of the hydrogels (Fig. 5E).

SUPPLEMENTARY MATERIALS

Supplementary material for this article is available at http://advances.sciencemag.org/cgi/content/full/4/6/eaat0098/DC1

fig. S1. Characterization of MXene ($Ti_3C_2T_x$) nanosheets.

fig. S2. Tensile fracture behaviors of pristine hydrogel.

fig. S3. Schematics of the uniformly dispersed polymer-clay network structure of M-hydrogel.
fig. S4. Experimental setup for electromechanical responses of M-hydrogel under compression.
fig. S5. Electromechanical response of M-hydrogel to vertical motion of object on its surface.
fig. S6. Anisotropic electric response of M-hydrogel to tensile and compressive strain.
fig. S7. Motion direction sensing comparison between the pristine hydrogel and M-hydrogel.
fig. S8. Mechanism of the speed-sensitive property of M-hydrogel.
fig. S9. Handwriting and vocal sensing performances of pristine hydrogel.
table S1. GF comparison between the M-hydrogel (4.1 wt %)–based sensor and recently reported hydrogel-based sensors.
movie S1. Stretchability and self-healability of M-hydrogel.
movie S2. Stretchability and self-healability of pristine hydrogel.
movie S3. Tensile fracture demonstration of M-hydrogel.
movie S4. Tensile fracture demonstration of pristine hydrogel.
movie S5. In situ TEM observation with varying tilt angle.
movie S6. In situ TEM observation with varying depth of focus.
References (*36*, *37*)

REFERENCES AND NOTES

1. A. Chortos, J. Liu, Z. Bao, Pursuing prosthetic electronic skin. *Nat. Mater.* **15**, 937–950 (2016).
2. Z. Lei, Q. Wang, S. Sun, W. Zhu, P. Wu, A bioinspired mineral hydrogel as a self-healable, mechanically adaptable ionic skin for highly sensitive pressure sensing. *Adv. Mater.* **29**, 1700321 (2017).
3. M. A. Darabi, A. Khosrozadeh, R. Mbeleck, Y. Liu, Q. Chang, J. Jiang, J. Cai, Q. Wang, G. Luo, M. Xing, Skin-inspired multifunctional autonomic-intrinsic conductive self-healing hydrogels with pressure sensitivity, stretchability, and 3D printability. *Adv. Mater.* **29**, 1700533 (2017).
4. J.-Y. Sun, C. Keplinger, G. M. Whitesides, Z. Suo, Ionic skin. *Adv. Mater.* **26**, 7608–7614 (2014).
5. C. Pang, G.-Y. Lee, T.-i. Kim, S. M. Kim, H. N. Kim, S.-H. Ahn, K.-Y. Suh, A flexible and highly sensitive strain-gauge sensor using reversible interlocking of nanofibers. *Nat. Mater.* **11**, 795–801 (2012).
6. L. Cai, L. Song, P. Luan, Q. Zhang, N. Zhang, Q. Gao, D. Zhao, X. Zhang, M. Tu, F. Yang, W. Zhou, Q. Fan, J. Luo, W. Zhou, P. M. Ajayan, S. Xie, Super-stretchable, transparent carbon nanotube-based capacitive strain sensors for human motion detection. *Sci. Rep.* **3**, 3048 (2013).
7. J. T. Muth, D. M. Vogt, R. L. Truby, Y. Mengüç, D. B. Kolesky, R. J. Wood, J. A. Lewis, Embedded 3D printing of strain sensors within highly stretchable elastomers. *Adv. Mater.* **26**, 6307–6312 (2014).
8. J. Cao, C. Lu, J. Zhuang, M. Liu, X. Zhang, Y. Yu, Q. Tao, Multiple hydrogen bonding enables the self-healing of sensors for human-machine interaction. *Angew. Chem. Int. Ed.* **56**, 8795–8800 (2017).
9. C. S. Boland, U. Khan, G. Ryan, S. Barwich, R. Charifou, A. Harvey, C. Backes, Z. Li, M. S. Ferreira, M. E. Möbius, R. J. Young, J. N. Coleman, Sensitive electromechanical sensors using viscoelastic graphene-polymer nanocomposites. *Science* **354**, 1257–1260 (2016).
10. Y. Wang, C. Zhu, R. Pfattner, H. Yan, L. Jin, S. Chen, F. Molina-Lopez, F. Lissel, J. Liu, N. I. Rabiah, Z. Chen, J. W. Chung, C. Linder, M. F. Toney, B. Murmann, Z. Bao, A highly stretchable, transparent, and conductive polymer. *Sci. Adv.* **3**, e1602076 (2017).
11. M. A. Gonzalez, J. R. Simon, A. Ghoorchian, Z. Scholl, S. Lin, M. Rubinstein, P. Marszalek, A. Chilkoti, G. P. López, X. Zhao, Strong, tough, stretchable, and self-adhesive hydrogels from intrinsically unstructured proteins. *Adv. Mater.* **29**, 1604743 (2017).
12. J. M. González-Dominguez, C. Martín, Ó. J. Durá, S. Merino, E. Vázquez, Smart hybrid graphene hydrogels: A study of the different responses to mechanical stretching stimulus. *ACS Appl. Mater. Interfaces* **10**, 1987–1995 (2017).
13. H. Liu, Y. Li, K. Dai, G. Zheng, C. Liu, C. Shen, X. Yan, J. Guo, Z. Guo, Electrically conductive thermoplastic elastomer nanocomposites at ultralow graphene loading levels for strain sensor applications. *J. Mater. Chem. C* **4**, 157–166 (2016).
14. H. Pang, C. Chen, Y.-C. Zhang, P.-G. Ren, D.-X. Yan, Z.-M. Li, The effect of electric field, annealing temperature and filler loading on the percolation threshold of polystyrene containing carbon nanotubes and graphene nanosheets. *Carbon* **49**, 1980–1988 (2011).
15. M. Naguib, V. N. Mochalin, M. W. Barsoum, Y. Gogotsi, 25th anniversary article: MXenes: A new family of two-dimensional materials. *Adv. Mater.* **26**, 992–1005 (2014).
16. M. Naguib, O. Mashtalir, J. Carle, V. Presser, J. Lu, L. Hultman, Y. Gogotsi, M. W. Barsoum, Two-dimensional transition metal carbides. *ACS Nano* **6**, 1322–1331 (2012).
17. M. Ghidiu, M. R. Lukatskaya, M.-Q. Zhao, Y. Gogotsi, M. W. Barsoum, Conductive two-dimensional titanium carbide 'clay' with high volumetric capacitance. *Nature* **516**, 78–81 (2014).
18. B. Anasori, M. R. Lukatskaya, Y. Gogotsi, 2D metal carbides and nitrides (MXenes) for energy storage. *Nat. Rev. Mater.* **2**, 16098 (2017).
19. Z. Ling, C. E. Ren, M.-Q. Zhao, J. Yang, J. M. Giammarco, J. Qiu, M. W. Barsoum, Y. Gogotsi, Flexible and conductive MXene films and nanocomposites with high capacitance. *Proc. Natl. Acad. Sci. U.S.A.* **111**, 16676–16681 (2014).
20. M. Boota, B. Anasori, C. Voigt, M.-Q. Zhao, M. W. Barsoum, Y. Gogotsi, Pseudocapacitive electrodes produced by oxidant-free polymerization of pyrrole between the layers of 2D titanium carbide (MXene). *Adv. Mater.* **28**, 1517–1522 (2016).
21. Y. Ma, N. Liu, L. Li, X. Hu, Z. Zou, J. Wang, S. Luo, Y. Gao, A highly flexible and sensitive piezoresistive sensor based on MXene with greatly changed interlayer distances. *Nat. Commun.* **8**, 1207 (2017).
22. Y. Cai, J. Shen, G. Ge, Y. Zhang, W. Jin, W. Huang, J. Shao, J. Yang, X. Dong, Stretchable $Ti_3C_2T_x$ MXene/carbon nanotubes composite based strain sensor with ultrahigh sensitivity and tunable sensing range. *ACS Nano* **12**, 56–62 (2018).
23. M. Alhabeb, K. Maleski, B. Anasori, P. Lelyukh, L. Clark, S. Sin, Y. Gogotsi, Guidelines for synthesis and processing of two-dimensional titanium carbide ($Ti_3C_2T_x$ MXene). *Chem. Mater.* **29**, 7633–7644 (2017).
24. L. Z. Zhao, C. H. Zhou, J. Wang, D. S. Tong, W. H. Yu, H. Wang, Recent advances in clay mineral-containing nanocomposite hydrogels. *Soft Matter* **11**, 9229–9246 (2015).
25. K. Haraguchi, R. Farnworth, A. Ohbayashi, T. Takehisa, Compositional effects on mechanical properties of nanocomposite hydrogels composed of poly(*N*,*N*-dimethylacrylamide) and clay. *Macromolecules* **36**, 5732–5741 (2003).
26. C.-W. Chang, A. van Spreeuwel, C. Zhang, S. Varghese, PEG/clay nanocomposite hydrogel: A mechanically robust tissue engineering scaffold. *Soft Matter* **6**, 5157–5164 (2010).
27. H. Zhang, H. Xia, Y. Zhao, Poly(vinyl alcohol) hydrogel can autonomously self-heal. *ACS Macro Lett.* **1**, 1233–1236 (2012).
28. M. R. Lukatskaya, S. Kota, Z. Lin, M.-Q. Zhao, N. Shpigel, M. D. Levi, J. Halim, P.-L. Taberna, M. W. Barsoum, P. Simon, Y. Gogotsi, Ultra-high-rate pseudocapacitive energy storage in two-dimensional transition metal carbides. *Nat. Energy* **2**, 17105 (2017).
29. Y.-J. Liu, W.-T. Cao, M.-G. Ma, P. Wan, Ultrasensitive wearable soft strain sensors of conductive, self-healing, and elastic hydrogels with synergistic "soft and hard" hybrid networks. *ACS Appl. Mater. Interfaces* **9**, 25559–25570 (2017).
30. J. J. Park, W. J. Hyun, S. C. Mun, Y. T. Park, O. O. Park, Highly stretchable and wearable graphene strain sensors with controllable sensitivity for human motion monitoring. *ACS Appl. Mater. Interfaces* **7**, 6317–6324 (2015).
31. G. Cai, J. Wang, K. Qian, J. Chen, S. Li, P. S. Lee, Extremely stretchable strain sensors based on conductive self-healing dynamic cross-links hydrogels for human-motion detection. *Adv. Sci.* **4**, 1600190 (2017).
32. K. Tian, J. Bae, S. E. Bakarich, C. Yang, R. D. Gately, G. M. Spinks, M. in het Panhuis, Z. Suo, J. J. Vlassak, 3D printing of transparent and conductive heterogeneous hydrogel-elastomer systems. *Adv. Mater.* **29**, 1604827 (2017).
33. S. Liu, L. Li, Ultrastretchable and self-healing double-network hydrogel for 3D printing and strain sensor. *ACS Appl. Mater. Interfaces* **9**, 26429–26437 (2017).
34. C. Wang, J. Zhao, C. Ma, J. Sun, L. Tian, X. Li, F. Li, X. Han, C. Liu, C. Shen, L. Dong, J. Yang, C. Pan, Detection of non-joint areas tiny strain and anti-interference voice recognition by micro-cracked metal thin film. *Nano Energy* **34**, 578–585 (2017).
35. X. Wang, Y. Gu, Z. Xiong, Z. Cui, T. Zhang, Silk-molded flexible, ultrasensitive, and highly stable electronic skin for monitoring human physiological signals. *Adv. Mater.* **26**, 1336–1342 (2014).
36. T. Hu, J. Wang, H. Zhang, Z. Li, M. Hu, X. Wang, Vibrational properties of Ti_3C_2 and $Ti_3C_2T_2$ (T = O, F, OH) monosheets by first-principles calculations: A comparative study. *Phys. Chem. Chem. Phys.* **17**, 9997–10003 (2015).
37. M. Hu, Z. Li, T. Hu, S. Zhu, C. Zhang, X. Wang, High-capacitance mechanism for $Ti_3C_2T_x$ MXene by in situ electrochemical raman spectroscopy investigation. *ACS Nano* **10**, 11344–11350 (2016).

Acknowledgments

Funding: Research reported in this publication is supported by King Abdullah University of Science and Technology (KAUST). **Author contributions:** Y.-Z.Z. and K.H.L. designed and conceptualized the project, designed the experiments, and analyzed the data. D.H.A. and R.S. conducted the TEM characterizations and 3D TEM tomography. Q.J. and H.K. synthesized and characterized the $Ti_3C_2T_x$ MXenes. H.N.A. supervised the overall conception and design of this project. All authors contributed to the writing of the paper. **Competing interests:** K.H.L., Y.-Z.Z., and H.N.A. are inventors on a provisional U.S. patent application related to this work (serial nos. 62/597,470 and 62/649,211, filed on 12 December 2017 and 28 March 2018). The other authors declare that they have no competing interest. **Data and materials availability:** All data needed to evaluate the conclusions in the paper are present in the paper and/or the Supplementary Materials. Additional data related to this paper may be requested from the authors.

Submitted 15 January 2018
Accepted 1 May 2018
Published 15 June 2018
10.1126/sciadv.aat0098

Citation: Y.-Z. Zhang, K. H. Lee, D. H. Anjum, R. Sougrat, Q. Jiang, H. Kim, H. N. Alshareef, MXenes stretch hydrogel sensor performance to new limits. *Sci. Adv.* **4**, eaat0098 (2018).

MXenes stretch hydrogel sensor performance to new limits

Yi-Zhou Zhang, Kang Hyuck Lee, Dalaver H. Anjum, Rachid Sougrat, Qiu Jiang, Hyunho Kim and Husam N. Alshareef

Sci Adv **4** (6), eaat0098.
DOI: 10.1126/sciadv.aat0098